Silica-magnesium-titanium Ziegler-Natta catalysts. Part 1: Structure of the pre-catalyst at a molecular level

Journal of Catalysis 424 (2023) 236–245

Contents lists available at ScienceDirect

Journal of Catalysis

journal homepage: www.elsevier.com/locate/jcat

Silica-magnesium-titanium Ziegler-Natta catalysts. Part 1: Structure of the pre-catalyst at a molecular level

Jelena Zarupski [a,d], Alessandro Piovano [a,d,1], Matteo Signorile [a], Alessia Amodio [a], Luca Olivi [b], Coen Hendriksen [c], Nicolaas H. Friederichs [c], Elena Groppo [a,d,*]

[a] Department of Chemistry, INSTM and NIS Centre, University of Torino, Via Giuria 7, 10125 Torino, Italy
[b] ELETTRA Sincrotrone Trieste, s.s. 14 km 163,500 in Area Science Park, Trieste I-34149, Italy
[c] SABIC Technology Center, 6167 RD Geleen, the Netherlands
[d] Dutch Polymer Institute, P.O. Box 902, 5600 AX Eindhoven, the Netherland

ARTICLE INFO

Article history:
Received 6 February 2023
Revised 17 May 2023
Accepted 25 May 2023
Available online 29 May 2023

ABSTRACT

In this paper, which is the first part of a more extended work, we elucidate the molecular level structure of a highly active SiO_2-supported Ziegler-Natta precatalyst obtained by reacting a dehydroxylated silica and a solution of an organomagnesium compound with $TiCl_4$. The synergetic combination of Ti K-edge and Ti L_3-edge X-ray Absorption spectroscopy (XAS) and diffuse reflectance UV–Vis spectroscopies, complemented by Density Functional Theory (DFT) simulations, indicate that small $TiCl_3$ clusters similar to β-$TiCl_3$ coexist with isolated monomeric Ti(IV) species. Ti K-edge Extended X-ray Absorption Fine Structure (EXAFS) Spectroscopy allows the quantification of these two phases and demonstrates that the Ti(IV) sites are 6-fold coordinated (either by six chlorine ligands or by five chlorine and one oxygen ligands), but highly distorted, similar to what is modelled for $TiCl_4$-capped $MgCl_2$ nanoplatelets. Finally, IR spectroscopy suggests that the $MgCl_2$ phase has a molecular character (Far-IR) and that the only accessible Mg^{2+} sites are uncoordinated cations acting as Lewis acid sites (IR of CO adsorbed at 100 K). Based on these experimental findings, we propose the co-existence in the precatalyst of small $TiCl_3$ clusters and of mixed oxo-chloride magnesium-titanium structures deposited at the silica surface. The evolution of the precatalyst in the presence of the activator and of the monomer is discussed in the second part of this work.

1. Introduction

Silica-supported titanium-based Ziegler–Natta (ZN) catalysts play a very important role in the polymerization of ethylene, notably in particle forming processes like gas-phase and slurry technologies. The first patents reporting the synthesis and catalytic performances of silica–magnesium–titanium catalysts date back to the beginning of the 1980s [1–3]. At that time, the adoption of silica carrier was envisioned as an alternative method with respect to ball-milling to make amorphous and disordered $MgCl_2$. Moreover, since the beginning it was also found that modifying the silica surface (for instance, by changing the calcination temperature) allowed to finely tune the polymer properties in terms of molecular weight distribution, evidently affecting the catalytic sites [4]. In particular, dehydroxylated silicas resulted in more performant catalysts, especially when chemically dehydrated, e.g., with hexamethyldisilazane [5]. This indicates that the silica is not only an inert carrier but plays a direct role in the definition of the active sites [2].

Although there exist many procedures to synthesize free-flowing silica–magnesium–titanium precatalysts highly active in ethylene (co)-polymerization, one of the most common consists in reacting (dehydroxylated) silica with solutions of organomagnesium compounds, which later can react with $TiCl_4$ [6-9]. Already in 1973 it was demonstrated by Haward and co-workers [10] that Grignard reagents (such as butyl magnesium halides, or dibutyl magnesium) in combination with an ether can completely reduce $TiCl_4$, to give soluble complexes of the type $TiCl_3$·$MgCl_2$·ether. These catalysts were more active by a factor of 3–10 compared to the first generation of ZN catalysts, prepared by reducing $TiCl_4$ with alkyl aluminum compounds [10]. Combination with silica also gave a better control on the particle size and morphology [11,12], making these catalysts very attractive for commercial use. Later on, it was also discovered that the incorporation of alcohols (e.g. 1-butanol) in the formulation gives lower molecular weight polyethylene, suggesting that alcohols act as efficient

* Corresponding author.
[1] Current address: GAME Lab, Department of Applied Science and Technology, Polytechnic of Torino, Corso Duca Degli Abruzzi, 24, 10129 Torino, Italy.

https://doi.org/10.1016/j.jcat.2023.05.024
0021-9517/

modifiers altering their chemical structure [1,13-15]. In particular, for catalysts obtained upon reacting dibutyl magnesium ($MgBu_2$) with $TiCl_4$, it was proposed that a primary function of alcohol is to scavenge alkyl aluminum that is usually added to increase $MgBu_2$ solubility in hydrocarbons, giving a product which does not substantially reduce $TiCl_4$ at 25 °C. In fact, trialkyl aluminum reagents classically react with alcohols liberating alkanes and generating alkoxides [10].

A comparison between alcohol-modified and alcohol-free silica-magnesium-titanium catalysts is reported in an early work of Hoff and co-workers [15], who investigated the effect of increasing amount of 1-butanol on both reactivity and polyethylene properties. They found that the butanol-modified catalysts give lower molecular weight and have reactivities slightly greater than the alcohol-free catalyst. In agreement with the role of alcohol discussed above, in the butanol-free catalyst 94% of the Ti is Ti(III) (as determined by titration), while the remaining is tetravalent. The room temperature EPR spectrum of the butanol-free precatalyst shows a single absorption at g = 1.948 value which does not change at 77 K, indicating the presence of a single type of EPR active Ti(III) species having restricted rotation. The percentage of Ti(III) in the precatalyst decreases almost linearly upon increasing the 1-butanol content, up to only 3.2% for BuOH/Mg = 2.0. At the same time, a second signal appears in the EPR spectra at about g = 1.97, which changes at 77 K and indicates the presence of at least one other form of Ti(III) with more freedom of rotation. The role of 1-butanol as a scavenger for the alkyl aluminum contained in $MgBu_2$ solution is further confirmed by the observation that, when it is added to the reaction mixture after $TiCl_4$ the fraction of Ti(III) remains very high (86%) [15].

As far as the role of 1-butanol in determining the structure of the Ti sites, no hypothesis are present in the pioneering work of Hoff and co-workers [15], but only the observation that neither the amount of Ti(III) nor that of Ti(IV) correlate with reactivity or melt index; the maximum reactivity and maximum melt index occurring for a BuOH/Mg ratio equal to 1. It is also important to notice that the precatalyst needs to be activated by alkyl aluminum compounds for developing activity in ethylene polymerization, which means that the Ti(III) species in the precatalyst are not alkylated or in any case not accessible to the monomer.

In this work we systematically investigate the properties of the best performing silica-magnesium-titanium precatalyst reported by Pullukat and Hoff [1] by means of a multi-technique approach comprising structural, electronic, and vibrational methods, complemented by DFT simulation. As previously demonstrated [16,17], a multi-technique spectroscopic investigation has the potential to clarify the mutual interactions among all the components constituting ZN catalysts, contributing to enhance their mechanistic understanding. For example, a multi-technique approach allowed unravelling the nature of the active $TiCl_x$ phase in model and industrial-like $MgCl_2$-supported catalysts [18–26], as well as in silica-supported ZN catalysts [27–35], both before [36,37] and after [23, 24] interaction with the alkyl aluminum activator. Herein, we confirm the co-presence of both Ti(III) and Ti(IV) species, as suggested in the early literature, in combination with small $MgCl_2$ clusters. Moreover, we determine the structure of the supported titanium chloride species at a molecular level and their accessibility to incoming probe molecules. The second part of this work [38] will focus on the role of the trialkyl aluminum activator in determining the properties of the titanium sites in the activated catalyst, as well as on the behaviour of the catalyst during ethylene polymerization. Altogether, the two parts of this work offer one of the most comprehensive studies on a class of heterogeneous catalysts with a huge industrial impact, but which are often left at the margins of interest of researchers involved in catalysts characterization.

2. Experimental

2.1. Precatalyst synthesis and reference samples

The ZN precatalyst was provided by SABIC and synthetized according to procedure described in US 4374753 patent [1]. Briefly, the synthesis consists in five subsequent steps. (1) SiO_2 (ES70X, specific surface area = 295 m^2/g, pore volume = 1.6 mL/g, average particle size 50 μm) was dried at 200 °C for 2 h under inert flow. (2) Dried silica was then chemically dehydroxylated by hexamethyldisilazane (HMDS) at 25 °C, followed by removal of unreacted HMDS and NH_3 by-product. 3) The so dehydroxylated silica was reacted with a heptane solution of dibutyl magnesium + trialkyl aluminum (TEAl), $MgBu_2$•x$AlEt_3$, Mg/Al = 6.1. In this regard, it is important to notice that neat $MgBu_2$ is an extended polymer [39,40] scarcely soluble in organic solvents, whose solubility can be increased upon addition of a small amount of alkyl aluminum compounds, which reduce the molecular weight by capping the $MgBu_2$ oligomers. Hence, the presence of TEAl in this synthetic mixture is unavoidable. 4) 1-butanol was added to the reaction mixture at 25 °C. 5) Finally, $TiCl_4$ was added, followed by drying at 90 °C to obtain free flowing powder. The amount of $MgBu_2$ complex was such that there was 0.8 mmol of $MgBu_2$ per gram of silica; the Mg/Ti molar ratio was set to 1.0 ± 0.1, resulting in 3.8 ± 0.2 wt% of Ti in the final catalyst.

Two reference samples have been measured along with the precatalyst: the β-$TiCl_3$ polymorph kindly donated by Prof. V. Busico (University of Naples); a $MgCl_2$-supported ZN precatalyst with dibutyl-phthalate (DBP) as internal donor was synthetized at JAIST and was object of an extensive characterization in our previous work [22,23]. The two reference samples will be referred to as β-$TiCl_3$ and ZNC(DBP), respectively.

2.2. Characterization methods

2.2.1. Ti K-edge X-ray absorption spectroscopy (XAS)

For the Ti K-edge X-ray Absorption Spectroscopy (XAS) measurements, the precatalyst sample was measured in the form of pellet, diluted in dehydrated boron nitride to optimize the Ti concentration in such a way that the edge jump was around 0.4, which is the best compromise between edge-jump and total absorption for this composition. Due to the air sensitivity, the pellet was done in the glovebox and sealed inside a Low-Density Polyethylene (LDPE) envelope under vacuum. The envelope with the pellet was mounted on the XAS sample-holder inside the glovebox. The sample holder was then extracted out of the glovebox, rapidly transferred to the measurement chamber at the beamline, and put under high vacuum. The whole procedure avoided exposure of the sample to air. A similar procedure was adopted for the two reference samples.

The measurements were performed at the XAS beamline at the Elettra Sincrotrone Trieste facility. The white beam was monochromatized using a Si(1 1 1) double crystal. Harmonic rejection was performed by detuning the second crystal of the monochromator of 50%. The spectra were acquired in transmission mode using ionization chambers for the detection of the reference and transmitted X-rays. A third ionization chamber recorded a Ti foil reference for energy calibration. The XAS spectra were recorded at the Ti K-edge with a beam size of ca. 6.0 × 1.5 mm (H × V). The energy range was scanned from 4700 to 6500 eV, with an energy step of 5 eV and an integration time of 1.2 s/point in the pre-edge region, 0.25 eV step and 2.0 s/point in the XANES region, and with a 3 eV step and an integration time that linearly increases as a function of k to account for the low signal-to-noise ratio at high k values in the Extended X-ray Absorption Fine Structure

(EXAFS) region. Each spectrum required an acquisition time of about 30 min.

The X-ray Absorption Near Edge Structure (XANES) spectra were aligned and normalized with the Athena software, by means of standard procedures. EXAFS data analysis was performed using the Arthemis software. The $k^2\chi(k)$ functions were Fourier transformed (FT) in the Δk = 2.0–10.0 $Å^{-1}$ interval. The fit was performed in R-space in the ΔR = 1.2–5.0 $Å^{-1}$ range. Phase and amplitudes were calculated by FEFF6.0 code.

2.2.2. Ti $L_{2,3}$-edge NEXAFS spectroscopy.

Ti $L_{2,3}$-edge Near Edge X-ray Absorption Fine Structure (NEXAFS) spectra were collected at the APE-HE beamline of the Elettra Sincrotrone Trieste facility, adopting the total electron yield (TEY) mode. To ensure the electrical conductivity, the samples in powder form were pressed inside a thin indium plate and fixed inside an ambient-pressure (AP) NEXAFS cell, which allows to perform measurements in the presence of gases [41]. This step was done inside a N_2-filled glove box to prevent contamination. The AP-NEXAFS cell was then inserted inside the high vacuum chamber of the APE-HE beamline and connected to a gas line, equipped with a liquid nitrogen trap to remove adventitious water contaminations. All the measurements were performed under a 5 mL min^{-1} He flow at 1 bar.

The spectra were collected with an energy step of 0.1 eV and an integration time per step of 0.18 s. The so collected data were processed using THORONDOR software [42].

2.2.3. DR UV–Vis-NIR spectroscopy

DR UV–vis spectra were collected with a Varian Cary5000 spectrophotometer, equipped with a diffuse reflectance sphere. The samples were measured in the powder form, inside a custom-made bulb cell in optical quartz (suprasil) filled inside the glovebox. The spectra were collected in reflectance mode (R%) and successively converted as Kubelka–Munk F(R) function. The precatalyst and ZNC(DBP) reference samples were measured undiluted, while β-$TiCl_3$ was diluted with dehydrated Teflon powder.

2.2.4. IR spectroscopy

Transmission IR spectra of the precatalyst were collected in both Mid-IR and Far-IR regions at a resolution of 2 cm^{-1} by means of a Bruker Vertex 70 spectrophotometer, equipped either with a MCT or a DTGS detector. In the Mid-IR region, the sample was measured in the form of a thin, self-supported, pellet, prepared in the glovebox and inserted into a custom-made cell allowing to perform measurements either under vacuum or in the presence of a controlled pressure of gases and at controlled temperature. CO adsorption at 100 K was performed as follows. After measuring the spectrum of the precatalyst at room temperature, CO was admitted in the cell at an equilibrium pressure P_{CO} = 50 mbar, and the temperature was slowly decreased by using liquid nitrogen. After reaching the CO saturation level, an IR spectrum was acquired. At that point, P_{CO} was decreased stepwise, and an IR spectrum was collected at each step by keeping the temperature constant. The IR spectra are shown after subtraction of that collected prior CO dosage.

For Far-IR measurements, the sample was measured in the form of a thin deposition on a silicon wafer using the same experimental strategy described in our previous work [24]. Briefly, the sample deposition was done in the glovebox and transferred into a custom-made cell equipped with two polyethylene windows, which allows performing the measurement without exposing the sample to air. The same procedure was applied for measuring β-$TiCl_3$.

2.3. Computational details

Calculations presented in this work have been performed by density functional theory (DFT) through the ORCA (v5.0.3) code [43]. The hybrid-GGA B3LYP functional [44,45] was adopted in conjunction with the Ahlrichs def2-TZVP basis set [46] for either geometry optimization and simulation of electronic spectra, namely optical, L_3-edge and K-edge absorption spectra. In the case of L_3- and K-edge spectra simulations, the zeroth order relativistic approximation (ZORA) [47] was included in the Hamiltonian to account for relativistic effects, expected to be relevant as the electronic transition involves core electrons in this type of spectroscopies. The specific ZORA-def2-TZVP(-f) basis set was preferred to the standard one for these specific simulations. Resolution of identity approximation was adopted to speed-up the calculations, adopting the general def2/J as auxiliary basis set (SARC/J for calculations including relativistic corrections).

Two minimal models, representative for Ti(III) in β-$TiCl_3$ and Ti (IV) supported on $MgCl_2$, where considered (Fig. 1): the former is constituted by a single chain of $TiCl_3$ featuring 6 Ti(III) atoms (formula Ti_6Cl_{18}); according to the literature, the single $TiCl_3$ chain has been treated with antiferromagnetic spin polarization [48]. The hexacoordinated Ti(IV) has been derived from that proposed in our previous publication and shown herein to better reproduce the isolated Ti(IV) species in a precatalyst [22], by decreasing the size of the $MgCl_2$ support to a minimal cluster with overall composition $TiMg_3Cl_{10}$. The computed electronic spectra were convoluted with Gaussian functions (FWMH = 1 eV for L- and K-edge, 0.5 eV for optical spectra), normalized in intensity per number of Ti atoms in the model and rescaled in energy with a multiplicative factor to match the experimental results (1.0690 for optical, 1.0271 for L_3-edge and 1.0088 for K-edge absorption spectra).

3. Results and discussion

3.1. Electronic properties: co-presence of isolated Ti(IV) and highly dispersed Ti(III) phase

Fig. 2 shows the Ti K-edge XAS, Ti $L_{2,3}$-edge NEXAFS and the DR UV–Vis-NIR spectra of the precatalyst, compared to those of the two reference compounds. Roughly speaking, the three techniques are all based on electronic excitations, but differ in the type of excited electrons (which depend on the energy of the incoming beam), while the arrival state is the same [49]. With Ti K-edge XAS, hard X-rays excite the Ti(*1s*) electrons, which are promoted either to localized states (unoccupied Ti(*3d*), Ti(*4p*) levels or Cl(π) levels, XANES region) or to the continuum (EXAFS region) [27,28,50]. In Ti $L_{2,3}$-edge NEXAFS, soft X-rays excite the Ti(*2p*) electrons to Ti(*3d*) levels [22,51]. Finally, in UV–Vis spectroscopy, photons in the UV region promote electron transfer from ligand-centred molecular orbitals (MOs) to Ti-centred MOs (charge-transfer transitions), while photons in the Vis range excite Ti(*3d*) electrons from filled to empty *3d* levels [17,22,52-54]. Since the electronic structure of the Ti sites depends on their local symmetry and oxidation state, it is clear that the three techniques offer complementary information on these two aspects.

Starting the discussion from the highest energy excitations, Fig. 2A shows the normalized Ti K-edge XANES spectra of the three samples. The spectrum of the SiO_2-supported precatalyst shows a weak pre-edge peak at 4968.8 eV (inset in Fig. 2A), which is not observed in the spectrum of β-$TiCl_3$, while is present in that of ZNC(DBP), although slightly shifted at higher energy. This peak is assigned to the Ti(*1s*) → Ti(*3pd*) localized transition, and is allowed only for titanium sites with a low symmetry and/or highly symmetric titanium sites but lacking the inversion centre (e.g. perfect

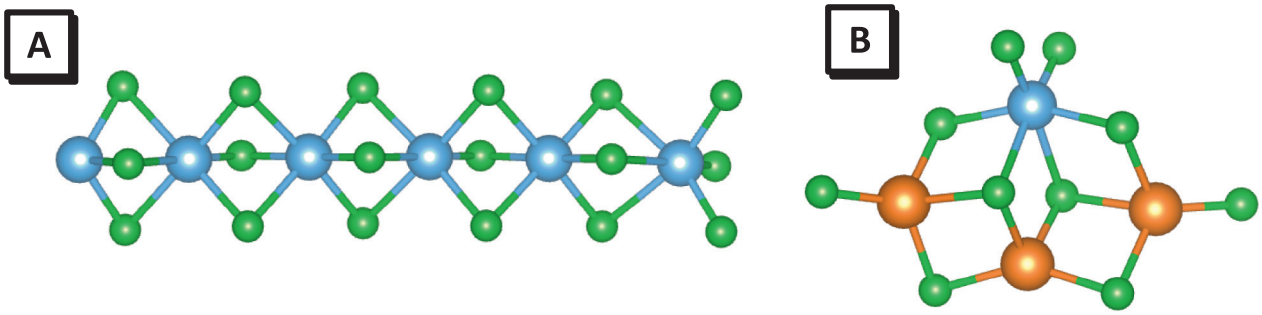

Fig. 1. The two minimal models adopted to simulate the electronic properties of Ti(III) in β-$TiCl_3$ (part A) and Ti(IV) supported on $MgCl_2$ (part B). Ti, Cl and Mg atoms are represented in blue, green and orange, respectively. (For interpretation of the references to colour in this figure legend, the reader is referred to the web version of this article.)

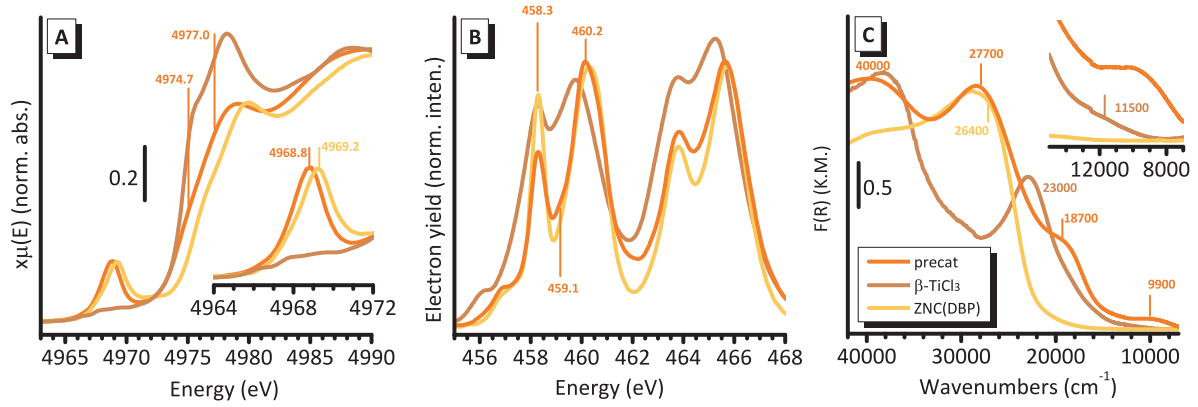

Fig. 2. Normalized Ti K-edge XANES spectra (part A), normalized Ti $L_{2,3}$-edge NEXAFS spectra (part b) and DR UV–Vis-NIR spectra (part C) of the SiO_2-supported precatalyst (orange), compared to those of β-$TiCl_3$ (brown) and ZNC(DBP) (yellow) reference samples. The inset in part A shows a magnification of the pre-edge peak, while that in part C highlights the region characteristic of d-d transitions. The main features of each spectrum are also indicated (for the assignment refer to the main text) and the colour code is the same in the three parts. (For interpretation of the references to colour in this figure legend, the reader is referred to the web version of this article.)

tetrahedral), while it is forbidden for titanium sites in an almost perfect octahedral symmetry (as in the case of β-$TiCl_3$). This assignment is confirmed by Fig. 3A, which shows the simulated Ti K-edge XANES spectra for two minimal models representative for Ti(III) in β-$TiCl_3$ and Ti(IV) supported on $MgCl_2$, the latter being characterized by a highly distorted geometry as predicted by machine learning-aided simulation for $TiCl_4$-capped $MgCl_2$ nanoplates [55]. Observation of the pre-edge peak in the spectra of the two precatalysts indicates that in both cases the majority of the titanium sites do not have a perfect octahedral symmetry, even though the low intensity (about 0.2 in normalized absorption) points toward high **coordination numbers** (e.g. distorted 6-fold or 5-fold coordination). In the "edge" region, the spectrum of the SiO_2-supported precatalyst shows a "double" absorption edge at 4974.7 and 4977.0 eV (evaluated as the maxima of the first derivative), which are assigned to Ti(*1s*) → Cl(*4p*) dipole-allowed transitions [17,28,50,56,57]. Similar features in the same position are observed also in the XANES spectrum of β-$TiCl_3$, but much more intense, because they are enhanced by the multiple scattering contributions arising from collinear Cl-Ti-Cl scattering paths, which are characteristic of Ti(III) sites in an almost perfect octahedral coordination. The energy position of these features indicates the presence of a Ti(III) phase in the SiO_2-supported precatalyst. For comparison, the spectrum of the ZNC(DBP) precatalyst is pretty similar to that of the SiO_2-supported precatalyst but shifted of ca. 1.4 eV, as expected in the presence of Ti(IV) species only. Notably, both the pre-edge and edge features together with the energy shift are well reproduced by the simulation on the two above mentioned models (Fig. 3A). The much lower intensity of the Ti (*1s*) → Cl(*4p*) features in the XANES spectrum of the SiO_2-supported precatalyst suggests that the multiple scattering contributions are limited, likely because the Ti(III) sites have lower symmetry.

Fig. 2B compares the Ti $L_{2,3}$-edge NEXAFS spectra of the three samples discussed so far, after normalization to the intensity of the second feature. It is worth noticing that the TEY acquisition mode renders the measurements highly surface sensitive, the probing depth being typically of a few nm. Generally speaking, a Ti 2*p* NEXAFS spectrum originates from the $2p^6 3d^n \rightarrow 2p^5 3d^{n+1}$ electronic transition; the L_3 edge corresponds to the $2p_{3/2}$ /excitations and is generally more defined than the L_2-edge, which originates from the $2p_{1/2}$ excitations. As widely discussed in our recent work [22], the $L_{2,3}$-edge is split into two main peaks that, within the molecular orbital picture for a Ti site in a distorted octahedral symmetry, are related to electronic transitions from the Ti 2*p* orbitals to the d_{t2g} and d_{eg} orbitals. Focusing the attention on the L_3 edge, the spectrum of the precatalyst is very similar to that of ZNC(DBP), with two main differences. 1) The peak associated to the d_{t2g} orbitals (at 458.3 eV) is less intense, which is expected in the presence of a fraction of Ti(III) sites. In fact, for Ti(III) sites the low-lying d_{t2g} orbitals are already occupied by one electron, hence the probability for this electronic transition is lower than for a Ti(IV) site, where the d_{t2g} orbitals are totally empty. 2) An additional weak peak is observed between the two main ones, at about 459.1 eV, which indicates the presence of a fraction of Ti (III) species [22]. These assignments, as well as the presence of a fraction of Ti(III) sites belonging to the β-$TiCl_3$ phase, are confirmed by simulated L-edge spectra shown in Fig. 3B. Interestingly, the

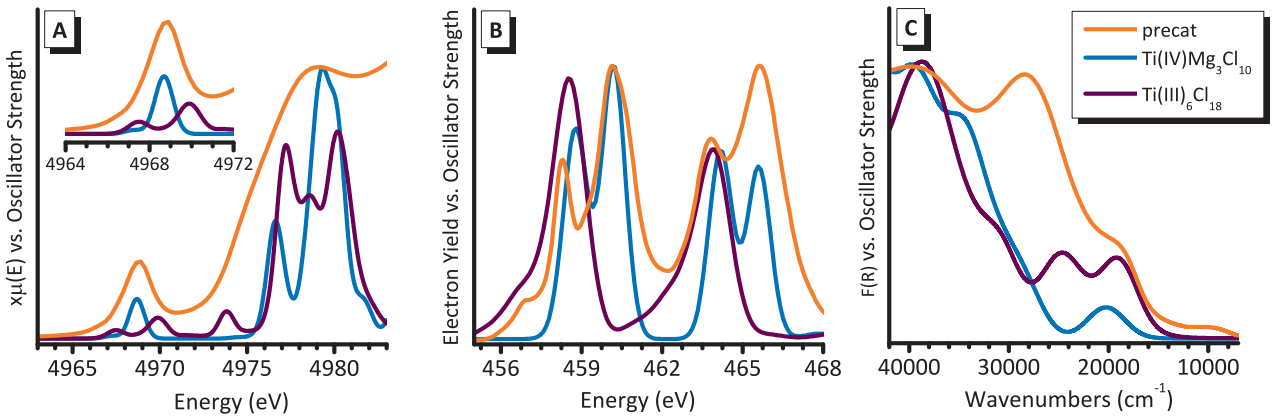

Fig. 3. Simulated Ti K-edge XANES (part A), Ti L_3-edge NEXAFS (part B) and UV–Vis (part C) spectra of two minimal models representative for β-$TiCl_3$ ($Ti(III)_6Cl_{18}$) and $MgCl_2$-supported Ti(IV) ($Ti(IV)Mg_3Cl_{10}$); the latter is the same employed as initial structural guess for EXAFS fit (*vide infra*). The simulated spectra are compared to the experimental one for the precatalyst.

spectrum for the $Ti(III)_6Cl_8$ model nicely matches the low energy components of the experimental NEXAFS spectrum of β-$TiCl_3$ (main peak at 458 eV and small shoulder at ca. 456 eV), whereas the second intense peak at higher energies (459.5 eV) is missing in the simulation. A possible explanation is the presence of impurities in the measured β-$TiCl_3$ sample (e.g. Al), that could alter the electronic features and the local environment around the absorbers.

Finally, to complete the description of the electronic properties of the Ti sites in the precatalyst, Fig. 2C shows the three DR UV–Vis-NIR spectra normalized to the intensity of the most intense band for a better comparison. The DR UV–Vis-NIR spectrum of the SiO_2-supported precatalyst is characterized by three main bands, at about 9900, 18700 and 27700 cm^{-1}, responsible for the brownish colour of the sample. The position and intensity of the absorption band at 9900 cm^{-1} indicate that it is due to a localized (Laporte forbidden, but spin allowed) $t_{2g} \rightarrow e_g$ *d-d* transition for Ti (III) sites in a distorted octahedral symmetry [58]. The energy position of the *d-d* absorption band (corresponding to the octahedral crystal field splitting, Δ_{CF}(UV)) depends on the type of ligand coordinated to the cation, according to the spectrochemical series. A band centred around 12,000 cm^{-1} was reported for hexahalotitanates, where the $TiCl_6^{-}$ anion is compensated by different cations; while crystal field splitting of about 19000 cm^{-1} is typical of a variety of O-bonded Ti(III) complexes [59]. A band as low as 10000 cm^{-1} was never reported for isolated Ti(III) sites, whereas a very weak band at about 11500 cm^{-1} is observed in the spectrum of β-$TiCl_3$ (inset in Fig. 2A). The energy position of the band at 19000 cm^{-1} is also typical for a *d-d* transition, but its intensity is anomalously high, since it approaches that of charge-transfer transitions. Similarly intense absorption bands occurring after the first spin-allowed transition and overlapping with other ligand-field bands up to the charge-transfer edge, have been reported for the α and β phases of $TiCl_3$ [17,22,53,60,61]; for example, a similar band is observed at 23000 cm^{-1} in the spectrum of β-$TiCl_3$. The most common interpretation is that of inter-site hopping transitions of the type $2(3d^1) \rightarrow 3d^0 + 3d^2$ involving two Ti(III) sites bridged by a common chloride ligand, and this is confirmed by our simulation, reported in Fig. 3C. Indeed, the natural transition orbitals analysis of acceptor states for these electronic transitions indicate that they are centred on vicinal Ti atoms bridged by chlorine ligands.

These two observations together corroborate the hypothesis that a fraction of the Ti sites in the precatalyst are in the form of small Ti(III) clusters resembling β-$TiCl_3$ (but not the same), whereby the Ti(III) are able to communicate each other by exchanging a *d* electron through bridging chloride ligands. In this respect it is worth remembering that, according to the pioneering works of Natta and co-workers [62], the chemical composition of the $TiCl_3$ phase obtained upon reaction of $TiCl_4$ with AlR_3 compounds strongly depends on the molar ratio: low Al/Ti molar ratio, as in the present case, should favour amorphous $TiCl_3$ products containing appreciable amounts of aluminum. A remaining fraction of Ti, however, is not reduced and accounts for the dominant band at 27700 cm^{-1}, where the spectrum of the clustered Ti(III) phase should have a minimum. Notably, this band falls in a very similar position to that observed in the spectrum of ZNC(DBP), which was assigned to ligand-to-metal charge-transfer transitions of the type Cl(π) → Ti(d_{t2g}) involving Ti(IV) sites in a (distorted) octahedral coordination [17,22,23,27,28,52–54]. The assignment is corroborated by the simulated UV–Vis spectrum for hexacoordinated Ti(IV) over $MgCl_2$, also reported in Fig. 3C. It is worth noting that the scarce reproduction of the relative intensities is due to the fact the experimental results have been obtained in reflectance mode, so that their intensity is affected by additional factors, such as a different penetration depth of the photons as a function of their energy and scattering-related phenomena due to the morphological features of the samples. Conversely, calculations approaches the optimal conditions achieved in transmission measurements, with a constant sampled volume and negligible scattering phenomena.

3.2. Local structure of the Ti sites

Additional information on the local structure of the Ti sites and on the surface species in the precatalyst come from FT-IR spectroscopy, in both Mid and Far-IR regions (Fig. 4A and B) and EXAFS spectroscopy (Fig. 5). Beside the bands characteristic of silica, the IR spectrum of the precatalyst shows a series of absorption bands assigned to the vibrational modes of alkyl chains, both in the stretching region (2000–2800 cm^{-1}) and in the bending region (1500–1350 cm^{-1}). In particular, the band at about 2970 cm^{-1} is indicative of the presence of -O-R species, likely -OBu species. Broad bands are also observed at 3660, 3500 and 3250 cm^{-1}, which indicate the presence of a few H-bonded –OH groups [63,64], despite the silica support was chemically dehydroxylated. Both -OBu and –OH surface species are clearly a consequence of the addition of 1-butanol during the synthesis.

In the Far-IR region (Fig. 4B), the only transparency window is below 350 cm^{-1}, since at higher wavenumbers SiO_2 contributes with very intense absorption bands. In that region, the spectrum of the precatalyst shows a very narrow band centred at

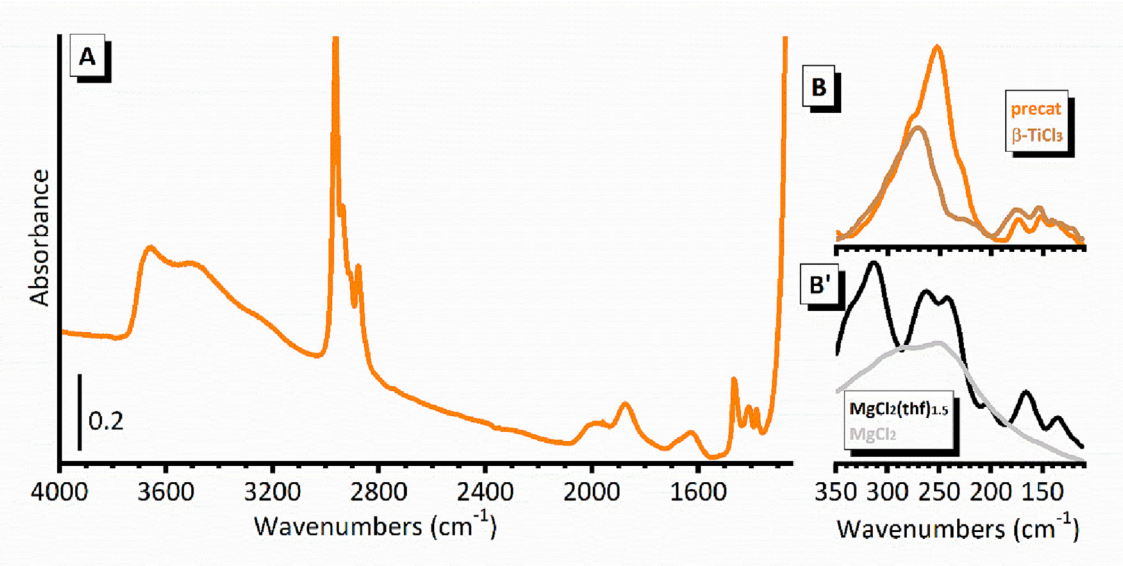

Fig. 4. Mid-IR (part A) and Far-IR (parts B and B') spectra of the precatalyst (orange), compared to those of β-$TiCl_3$ (dark yellow), $MgCl_2(thf)_{1.5}$ [53] (black) and ball-milled $MgCl_2$ (gray) [24] reference samples. (For interpretation of the references to colour in this figure legend, the reader is referred to the web version of this article.)

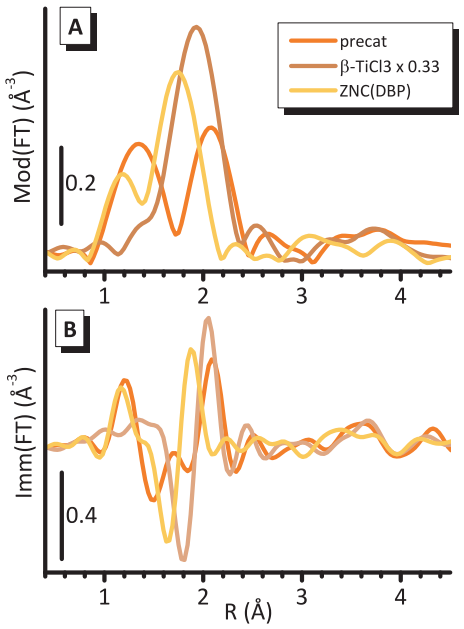

Fig. 5. k^2-weighted |FT| (part A) and Imm(FT) (part B) of the EXAFS function for the precatalyst, compared to those of β-$TiCl_3$ and ZNC(DBP) as references. It is worth noticing that the spectrum of β-$TiCl_3$ has been divided by three for a better comparison.

252 cm^{-1}, with a tail at 277 cm^{-1} and a triplet of weaker bands in the 210–120 cm^{-1} range. The latter features are very similar to those observed in the spectrum of β-$TiCl_3$ (brown spectrum in Fig. 4B), which confirms the DR UV–Vis-NIR results. The very narrow band at 252 cm^{-1}, instead, falls in a region characteristic for ν(Mg-Cl_{bridge}) vibrations involving bridging chlorine species. For comparison, Fig. 4B' shows the Far-IR spectra of two reference compounds, previously reported in the literature, namely the $MgCl_2(thf)_{1.5}$ molecular complex [53] and a ball-milled $MgCl_2$ sample characterized by crystals of nanometric dimension [24] (black and grey spectra, respectively). It is evident that the full-width-at-half-maximum of the ν(Mg-Cl_{bridge}) band is very narrow for the molecular complex, while the same vibration for bulk $MgCl_2$ gives rise to a very broad band extending in the whole 350 – 140 cm^{-1} region. The spectrum of $MgCl_2(thf)_{1.5}$ shows also a narrow band centred at 312 cm^{-1}, which is attributed to the ν(Mg-$Cl_{terminal}$) vibration of terminal chlorine species. Hence, the Far-IR spectrum proves that the $MgCl_2$ phase in the precatalyst has a molecular character, very much similar to that displayed for example by the $MgCl_2(thf)_{1.5}$ complex, where bridged Mg-Cl-Mg chlorine species dominate over the terminal Mg-Cl ones. We speculate that these $MgCl_2$ "quantum dots", formed during reaction of $MgBu_2$ with $TiCl_4$ in the presence of 1-butanol, are stabilized not only by adsorbed titanium chlorides, but also by the surface butoxide groups which act as capping functional groups.

Ti K-edge EXAFS spectroscopy, which is element selective, allows us to clarify which is, in average, the local structure of the titanium sites. Fig. 5A shows the modulus of the Fourier-Transformed k^2-weighted EXAFS function of the precatalyst, compared to those of β-$TiCl_3$ (divided by a factor of 3) and ZNC(DBP) references, while Fig. 5B shows the corresponding imaginary parts. A first relevant observation is that the spectrum of the precatalyst, as well as that of ZNC(DBP), are much weaker than that of crystalline β-$TiCl_3$, approximately 1/3. This is clearly not explainable only by considering smaller coordination numbers in the titanium coordination sphere (which would mean less than 3 ligands per each titanium sites) and/or a reduced dimensionality of the titanium phase. A similar behaviour was previously reported by some of us for both unsupported and silica-supported ZN catalysts synthetized from tetrahydrofuranate precursors [17,27,28,50,53], and explained as due to the presence of several ligands at similar distances in titanium coordination sphere, whose contributions are at least partially out-of-phase. A second important observation is that the spectrum of the precatalyst shows two peaks at 1.35 and 2.07 Å (phase-uncorrected) separated by a dip, in contrast to that of β-$TiCl_3$, which shows a single intense peak at 1.93 Å. ZNC(DBP) has an intermediate behaviour, since it shows a dominant peak at 1.74 Å, with a shoulder at 1.19 Å, more visible in the imaginary part. These differences clearly indicate that the local structure around the titanium sites is not the same in the three cases. A rigorous fit of the EXAFS signal for both the SiO_2-supported and ZNC (DBP) precatalysts is made difficult by the relatively short k-range that can be safely used in the analysis, by the co-presence in the titanium coordination sphere of several ligands contributing at similar distance but partially out-of-phase and, for the SiO_2-

supported precatalyst, also by the co-presence of at least two structurally different titanium phases (as demonstrated in previous section).

The EXAFS data analysis for the precatalyst was performed through a two-phase two-step fit. The optimized parameters are summarized in Table 1, while Fig. 6 shows the two best fits and the most relevant scattering paths contributing to the fit. At first, the fraction of Ti(III) in the form of $TiCl_3$ clusters was determined by fitting the 2.2–5.0 Å region, which is dominated by the multiple scattering (MS) contributions of collinear Cl-Ti-Cl scattering paths. It accounts for 41% of the total ("fraction" in Table 1), and is in very well agreement with the early paper of Hoff et al. [15], where the percentage of Ti(III) in a precatalyst with similar composition was estimated by titration to be 43% of the total. The first shell average Ti-Cl distance for this Ti(III) phase is that typical of $TiCl_3$ polymorphs (2.48 ± 0.02 Å), with a slightly large Debye-Waller factor (0.010 ± 0.008 $Å^2$) probably induced by the small size and heterogeneity of the clusters. In the second step, the structural parameters related to the $TiCl_3$ phase were fixed, and a first shell fit of the remaining 59% of titanium was attempted. Reasonable fits were obtained only upon including three different Ti-Cl contributions at short, medium, and long distances (Cl_s, Cl_m and Cl_l, respectively), as suggested by the Ti(IV)Mg_3Cl_{10} DFT optimized model. Interestingly, this is also the case for Ti(IV) sites in a series of

Table 1
Optimized parameters in the analysis of the EXAFS spectrum for the SiO_2-supported precatalyst according to two different structural models.[a]

	Ligand	N[d]	ΔE (eV)	Fraction[e]	R (Å)[f]	σ^2 ($Å^2$)	R_{factor}
FIT1[b]	Cl_s	2	−2.1 ± 0.5	0.59	2.105 ± 0.014 (2.170 ± 0.001)	0.010 ± 0.003	0.022
	Cl_m	2			2.279 ± 0.013 (2.372 ± 0.005)	0.009 ± 0.003	
	Cl_l	2			2.67 ± 0.04 (2.75 ± 0.03)	0.034 ± 0.010	
	$Cl_{cluster}$	6		0.41	2.48 (2.44 ± 0.13)	0.010	
FIT2[c]	O	1	−1.6 ± 0.6	0.59	1.827 ± 0.058	0.006 ± 0.010	0.017
	Cl_s	1			2.099 ± 0.118	0.014 ± 0.030	
	Cl_m	2			2.239 ± 0.030	0.011 ± 0.007	
	Cl_l	2			2.70 ± 0.057	0.034 ± 0.008	
	$Cl_{cluster}$	6		0.41	2.48	0.010	

[a] $N_{ind} = 2\Delta k \Delta R/\pi > 10$.
[b] FIT 1 was performed by considering the contribution of three couples of chlorine ligands around the absorber, each couple characterized by a different Ti-Cl distance (short, medium, and long).
[c] FIT 2 was performed by considering the contribution of five chlorine ligands (1 at short, 2 at medium and 2 at long distance) and one oxygen ligand.
[d] The coordination numbers were fixed to those of the models, while the amplitude reduction factor S_0^2 was fixed to that obtained by fitting the data of $TiCl_3$ reference compounds ($S_0^2 = 0.8$).
[e] The fraction × of Ti(III) in the form of $TiCl_3$ clusters was determined by fitting the 2.2–5.0 Å region; the fraction of the remaining Ti(IV) sites was fixed as (1 − x).
[f] Average Ti-Cl distances determined form DFT are reported in brackets.

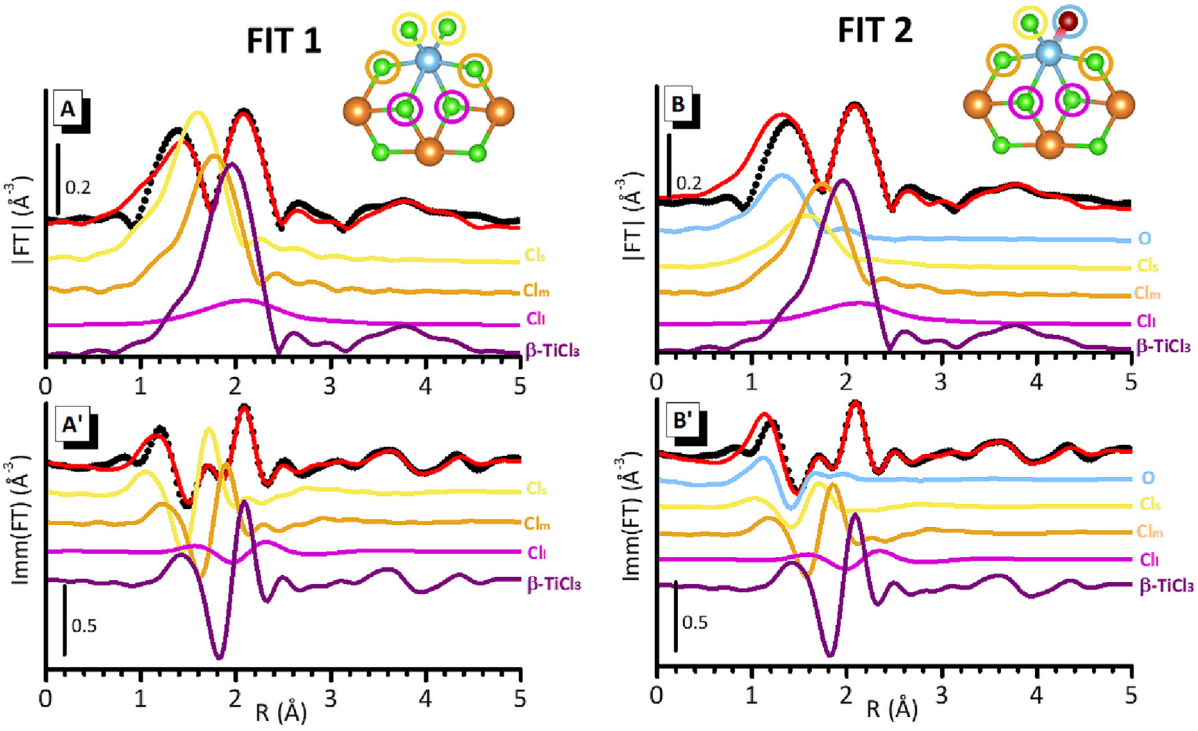

Fig. 6. Analysis of the EXAFS spectrum for the SiO_2-supported precatalyst. Parts A and A': FIT1, which includes the contribution of only chlorine ligands. The experimental phase-uncorrected FT of the $k^2\chi(k)$ EXAFS function is shown in both modulus and imaginary parts (dotted curves in parts A and B respectively), overlapped to the result of the fit (red lines). The relevant scattering paths are also shown, vertically translated for clarity. Parts B and B': same as parts A and A', for FIT2, which includes the contributions of an oxygen ligand instead of a chlorine at short distance. The inset in part A shows the model used in FIT1, as reported in Ref. [55], while that in part B has been obtained from the previous one upon substituting a Cl_s ligand with an oxygen (of a butoxide moiety). Ti, Cl, Mg and O atoms are represented in blue, green, orange and red, respectively. (For interpretation of the references to colour in this figure legend, the reader is referred to the web version of this article.)

machine learning-aided models of $TiCl_4$-capped $MgCl_2$ nanoplates, where the six chlorine ligands around Ti(IV) sites can be classified in three couples with different Ti-Cl distances, being the terminal chlorine species at shorter distance than the bridged ones [55]. Two equally good fits (FIT1 and FIT2 in Table 1) were obtained, either considering 6 chlorine ligands (FIT1), or 5 chlorine and 1 oxygen (FIT2), the latter model having been stimulated by the observation of abundant alkoxy species at the catalyst surface. Both situations are compatible with the results discussed so far and suggest that, beside the highly dispersed $TiCl_3$ phase, the remaining 60% of the titanium is present as monomeric Ti(IV), with a distorted octahedral symmetry determined mainly by chlorine ligands, but possibly also by one butoxide ligand. The fitted Ti-Cl distances for FIT1 are in good agreement with the DFT results, further supporting the reliability of the structural hypothesis for the Ti(IV) sites.

In this respect, the presence of alkoxy ligands in the Ti coordination sphere of ZN catalysts has been object of discussion in the specialized literature. In fact, one of the most common preparation routes for industrial ZN catalysts, i.e. the conversion of a $Mg(OEt)_2$ precursor to $MgCl_2$ by reaction with $TiCl_4$ in the presence of an internal donor (ID) [37], is known to produce titanium ethoxy compounds of the type $TiCl_{4-x}(OEt)_x$, which may remain adsorbed at the catalyst surface as impurities [65]. This is similar to what is proposed here for the butoxide ligands generated during the catalyst synthesis. The role of these alkoxy ligands in olefin polymerization catalysis has been questioned since long time, and so far, a definite answer has not been achieved yet. However, several independent experimental observation point toward a negative correlation between the alkoxy content and the catalyst performance (both in terms of activity and stereoregularity of the polypropylene produced) [66–68]. This was recently confirmed by a systematic work from Taniike and co-workers [69], who concluded that titanium alkoxy compounds are poisonous by-products of ZN catalysts for PP production, increasing the amorphous fraction of the polymer and decreasing the stereoregularity of the remaining highly crystalline fraction.

3.3. Accessibility of the surface sites

Finally, the accessibility of the surface sites at molecular level has been investigated by means of IR spectroscopy of CO adsorbed at 100 K, as successfully reported in the literature for different classes of high-surface area materials [70–72], including polyolefin catalysts [20,24,73–77]. CO was chosen as a probe molecule since it is a soft base able to specifically probe surface sites of different strength [72,78]. Moreover, CO was confirmed to be a good probe molecule for different model $MgCl_2$-supported ZN catalysts [18,20,24,25,73,74] as well as for SiO_2-supported ZN catalysts [27,29].

Fig. 7 shows the FT-IR spectra (in the ν(CO) region) of CO adsorbed at 100 K on the precatalyst after subtraction of the spectrum collected prior CO dosage, as a function of the CO coverage. The spectrum collected at θ_{max} is characterized by three intense and sharp bands at 2136, 2155, and 2181 cm^{-1}, which behave differently as a function of the equilibrium pressure (P_{CO}). The band at 2136 cm^{-1} is the first one to disappear upon decreasing P_{CO}, indicating a weak interaction, and is attributed to physisorbed CO [70]. Also, the band at 2155 cm^{-1} decreases in intensity quite rapidly upon decreasing the CO coverage, almost without shifting, and is attributed to CO adsorbed on rather weak Lewis acid sites [79]. A band in a similar position was observed upon CO adsorption at 100 K on bare $MgCl_2$, and is ascribed to CO on 5-fold coordinated Mg^{2+} cations [18,20]. In contrast, the band at 2181 cm^{-1} is more resistant to degassing and shifts up to 2186 cm^{-1} at the lowest CO coverage. This band can be ascribed to CO adsorbed on stronger

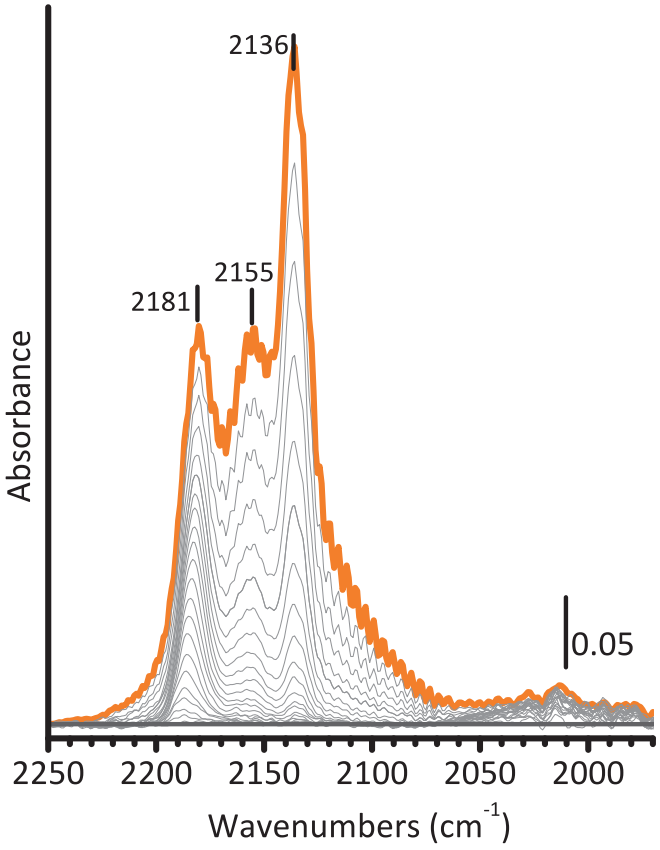

Fig. 7. FT-IR spectra (in the ν(CO) region) of CO adsorbed at 100 K on the precatalyst as a function of CO coverage Θ (from Θ_{max} in orange colour to zero in dark grey). The spectra are shown after subtraction of the spectrum prior the dosage of CO. (For interpretation of the references to colour in this figure legend, the reader is referred to the web version of this article.)

Lewis acid sites, as previously reported for CO on 4-fold coordinated Mg^{2+} cations [18,20]. Importantly, no bands are observed around 2100 cm^{-1}, where CO in interaction with Ti(III) sites should contribute [25,73,80]. This indicates that the Ti(III) sites present in the SiO_2-supported precatalyst are not accessible to incoming molecules.

Overall, this result is in very well agreement with the scenario obtained with the other characterization techniques, which demonstrated that both the Ti(IV) and the Ti(III) sites are 6-fold coordinated, and hence do not display a coordination vacancy available for CO coordination.

4. Conclusions

Herein we reported a detailed investigation of the physicochemical properties of a Ziegler-Natta precatalyst, selected as a prototype for the family of silica-supported ZN catalysts prepared by reacting dehydroxylated silica with a solution of an organomagnesium compound and $TiCl_4$. These catalysts are largely employed in fluidized-bed gas-phase ethylene polymerization, which is one of the polymerization technologies most applied worldwide. Although developed in the 1980s, the specialized literature does not report any hypothesis on the structure of the catalyst at a molecular level, but only a few observations on the co-presence of both Ti(IV) and Ti(III) species, in a relative amount which depends on the catalyst composition, but that does not correlate neither with the activity nor with the properties of the produced polyethylene.

By synergically coupling a series of advanced characterization methods complemented by DFT simulations we have been able to disclose the structural, electronic, and vibrational properties of the precatalyst at a molecular level. We confirmed the co-presence of both Ti(III) and Ti(IV) species, whose relative concentration is in very well agreement with that determined by titration in the early work of Hoff et al. [81]. We found that the Ti (III) species have electronic properties similar to those of Ti(III) in the β-$TiCl_3$ polymorph, but they are highly dispersed. The Ti (IV) sites, instead, are monomeric and surrounded mostly by chlorine ligands, but possibly also by one butoxide ligand, with a distorted octahedral symmetry characterized by at least three different Ti-ligand distances. Both Ti(III) and Ti(IV) species are inter-connected with nanometric $MgCl_2$ seeds having a molecular character, which are at least partially stabilized also by butoxide moieties. The only sites of these molecular clusters which are accessible to CO as molecular probe are uncoordinated Mg^{2+} cations. Regarding the interaction of these nanometric clusters with the silica surface, they are probably simply deposited on it. In fact, we do expect that the silica surface dehydroxylated by HMDS contains a very low amount of free silanols, as well as siloxane bridges, which are known to be the surface species reactive towards MgR_2, AlR_3 and $TiCl_4$ reagents.

At a more general level, the results reported in this work demonstrate the potential of a multi-technique approach in unravelling the molecular structure of complex industrially relevant catalysts synthetized by reacting together many components and constituted by multiple phases. As the follow-up, the silica-supported ZN catalysts obtained upon activation of here studied precatalyst with alkyl aluminum were investigated by applying the same spectroscopic approach also under polymerization working conditions [38].

Data availability

Data will be made available on request.

Declaration of Competing Interest

The authors declare that they have no known competing financial interests or personal relationships that could have appeared to influence the work reported in this paper.

Acknowledgments

This work forms part of the research program of DPI, project #813. The authors acknowledge support from Project CH4.0 under MUR (Italian Ministry for the University) program "Dipartimenti di Eccellenza 2023-2027" (CUP: D13C22003520001).

References

[1] T.J. Pullukat, R.E. Hoff, Polymerization Catalyst and Method, US Patent 4374753, 1983.
[2] M. Shida, T.J. Pullukat, R.E. Hoff, Polymerization catalysts, US Patent 4263171, 1981.
[3] T.E. Nowlin, K.P. Wagner, Highly active catalyst composition for polymerizing alfa-olefins, US Patent 4481301, 1984.
[4] H. Teimoury, N. Moeini, N. Bahri-Laleh, F.Y. Shih, M.V. Varnoosfaderani, The effect of SiO_2 calcination temperature and [Si]/[Mg] molar ratio on the performance of bi-supported Ziegler-Natta catalysts in ethylene polymerizations, J. Polym. Res. 30 (2023).
[5] T. Garoff, S. Johansson, U. Palmqvist, D. Lindgren, M. Stuela, P. Waldvogel, A. Kostiainen, Procatalyst for ethylene polymer production, method for its preparation and use, EP Patent 0688794A1, 1995.
[6] J.P. Blitz, C.C. Meverden, R.E. Diebel, Reactions of Dibutylmagnesium with Modified Silica Gel Surfaces, Langmuir 1122–1129 (1998) 14.
[7] R.O. Hagerty, I.B. Petsche, K.G. Schurzky, Alpha-Olefins Polymerization Catalysts of High Productivity, US Patent 4562169, 1985.
[8] H.L. Hsieh, M.P. McDaniel, J.L. Martin, P.D. Smith, D.R. Fahey, Polyolefin catalysts based on titanium and vanadium chlorides, in: R.B. Seymour, T. Cheng (Eds.), Advances in Polyolefins: The World's Most Widely Used Polymers, 1st ed.,., Springer Science, 1987, pp. 153–170.
[9] J.P. Blitz, Model silica supported olefin polymerization catalysts, in: T.C. Chung (Ed.), New Advances in Polyolefins, 1st ed., Springer Science, New York, 1993, pp. 1–14.
[10] R.N. Haward, A.N. Roper, K.L. Fletcher, Highly active catalysts for ethylene polymerization by the reduction of $TiCl_4$, with organomagnesium compounds, Polymer 14 (1973) 365–372.
[11] A. Muroz-Escalona, J.G. Hernandez, J.A. Gallardo, Catalytic activity and control of the nascent morphology of polyethylenes obtained with first and second generation of Ziegler-Natta catalysts, J. Appl. Polym. Sci. 29 (1984) 1187–1202.
[12] A. Muroz-Escalona, J.G. Hernandez, Particle control of supported Ziegler-Natta catalysts, in: R.B. Seymour, T. Cheng (Eds.), Advances in Polyolefins: The World's Most Widely Used Polymers, first ed., Springer Science, New York, 1987, pp. 179–202.
[13] R.A. Dombro, Polymerization Method, US Patent 4458058, 1984.
[14] R.E. Hoff, Polymerization Catalyst and Method, US Patent 4402861, 1983.
[15] R.E. Hoff, T.J. Pullukat, R.A. Dombro, Alcohol-modified magnesium titanium catalysts, in: R.B. Seymuor, T. Cheng (Eds.), Advances in Polyolefins: The Worlds's Most Widely Used Polymers, first ed., Springer Science, New York, 1987, pp. 241–254.
[16] A. Piovano, E. Groppo, Flexible ligands in heterogeneous catalysts for olefin polymerization: Insights from spectroscopy, Coord. Chem. Rev. 451 (2022).
[17] E. Groppo, K. Seenivasan, C. Barzan, The potential of spectroscopic methods applied to heterogeneous catalysts for olefin polymerization, Catal Sci. Technol. 3 (2013) 858–878.
[18] A. Piovano, M. D'Amore, K.S. Thushara, E. Groppo, Spectroscopic evidences for TiCl4/donor complexes on the surface of $MgCl_2$-supported ziegler-natta catalysts, J. Phys. Chem. C. 122 (2018) 5615–5626.
[19] K.S. Thushara, M. D'Amore, A. Piovano, S. Bordiga, E. Groppo, The influence of alcohols in driving the morphology of magnesium chloride nanocrystals, ChemCatChem 9 (2017) 1782–1787.
[20] M. D'Amore, K.S. Thushara, A. Piovano, M. Causà, S. Bordiga, E. Groppo, Surface investigation and morphological analysis of structurally disordered $MgCl_2$ and $MgCl_2/TiCl_4$ Ziegler-Natta Catalysts, ACS Catal. 6 (2016) 5786–5796.
[21] M. Milanesi, A. Piovano, T. Wada, J. Zarupski, P. Chammingkwan, T. Taniike, E. Groppo, Influence of the synthetic procedure on the properties of three Ziegler-Natta catalysts with the same 1,3-diether internal donor, Catal Today. 418 (2023).
[22] A. Piovano, M. Signorile, L. Braglia, P. Torelli, A. Martini, T. Wada, G. Takasao, T. Taniike, E. Groppo, Electronic properties of Ti sites in Ziegler-Natta catalysts, ACS Catal. 11 (2021) 9949–9961.
[23] A. Piovano, T. Wada, A. Amodio, G. Takasao, T. Ikeda, D. Zhu, M. Terano, P. Chammingkwan, E. Groppo, T. Taniike, Formation of highly active ziegler-natta catalysts clarified by a multifaceted characterization approach, ACS Catal. 11 (2021) 13782–13796.
[24] A. Piovano, M. D'Amore, T. Wada, P. Cleto Bruzzese, G. Takasao, A. Thakur, P. Chammingkwan, M. Terano, B. Civalleri, S. Bordiga, T. Taniike, E. Groppo, Revisiting the identity of δ-$MgCl_2$: Part II. Morphology and exposed surfaces studied by vibrational spectroscopies and DFT calculation, J. Catal. 387 (2020) 1–11.
[25] P. Pletcher, A. Welle, A. Vantomme, B.M. Weckhuysen, Quality control for Ziegler-Natta catalysis via spectroscopic fingerprinting, J. Catal. 363 (2018) 128–135.
[26] E. Morra, E. Giamello, S. Van Doorslaer, G. Antinucci, M. D'Amore, V. Busico, M. Chiesa, Probing the coordinative unsaturation and local environment of Ti3+ sites in an activated high-Yield Ziegler-Natta catalyst, Angew. Chem. Int. Ed. 54 (2015) 4857–4860.
[27] E. Groppo, K. Seenivasan, E. Gallo, A. Sommazzi, C. Lamberti, S. Bordiga, Activation and in situ ethylene polymerization on silica-supported Ziegler-Natta catalysts, ACS Catal. 5 (2015) 5586–5595.
[28] K. Seenivasan, E. Gallo, A. Piovano, J.G. Vitillo, A. Sommazzi, S. Bordiga, C. Lamberti, P. Glatzel, E. Groppo, Silica-supported Ti chloride tetrahydrofuranates, precursors of Ziegler-Natta catalysts, Dalton Trans. 42 (2013) 12706–12713.
[29] A. Piovano, G.A. Martino, C. Barzan, A spectroscopic investigation of silica-supported TiClx species: a case study towards Ziegler-Natta catalysis, Rend. Lincei. Sci. Fis. Nat. 28 (2017) 43–49.
[30] A. Yakimov, J. Xu, K. Searles, W.C. Liao, G. Antinucci, N. Friederichs, V. Busico, C. Copéret, DNP-SENS formulation protocols to study surface sites in Ziegler-Natta catalyst MgCl2 supports modified with internal donors, J. Phys. Chem. C 125 (2021) 15994–16003.
[31] F. Allouche, D. Klose, C.P. Gordon, A. Ashuiev, M. Wörle, V. Kalendra, V. Mougel, C. Copéret, G. Jeschke, Low-coordinated titanium(III) alkyl—molecular and surface—complexes: detailed structure from advanced EPR spectroscopy, Angew. Chem. Int. Ed. 57 (2018) 14533–14537.
[32] A. Ashuiev, M. Humbert, S. Norsic, J. Blahut, D. Gajan, K. Searles, D. Klose, A. Lesage, G. Pintacuda, J. Raynaud, V. Monteil, C. Copéret, G. Jeschke, Spectroscopic signature and structure of the active sites in Ziegler-Natta polymerization catalysts revealed by electron paramagnetic resonance, J. Am. Chem. Soc. 143 (2021) 9791–9797.
[33] A.V. Cheruvathur, E.H.G. Langner, J.W.H. Niemantsverdriet, P.C. Thüne, In Situ ATR-FTIR studies on MgCl 2-diisobutyl phthalate interactions in thin film ziegler-natta catalysts, Langmuir 28 (2012) 2643–2651.

[34] E. Grau, A. Lesage, S. Norsic, C. Copéret, V. Monteil, P. Sautet, Tetrahydrofuran in $TiCl_4$/THF/$MgCl_2$: a non-innocent ligand for supported Ziegler-Natta polymerization catalysts, ACS Catal. 3 (2013) 52–56.
[35] V. D'Anna, S. Norsic, D. Gajan, K. Sanders, A.J. Pell, A. Lesage, V. Monteil, C. Copéret, G. Pintacuda, P. Sautet, Structural characterization of the EtOH-$TiCl_4$-$MgCl_2$ Ziegler-Natta precatalyst, J. Phys. Chem. C 120 (2016) 18075–18087.
[36] E.S.M. Blaakmeer, G. Antinucci, A. Correa, V. Busico, E.R.H. Van Eck, A.P.M. Kentgens, Structural Characterization of Electron Donors in Ziegler-Natta Catalysts, J. Phys. Chem C 122 (2018) 5525–5536.
[37] T. Taniike, T. Funako, M. Terano, Multilateral characterization for industrial Ziegler-Natta catalysts toward elucidation of structure–performance relationship, J Catal. 311 (2014) 33–40.
[38] J. Zarupski, A. Piovano, M.J. Werny, A. Martini, L. Braglia, P. Torelli, C. Hendriksen, N.H. Friederich, F. Meirer, B.M. Weckhuysen, Elena Groppo, Silica-magnesium-titanium Ziegler-Natta catalysts. Part 2. Properties of the active sites and fragmentation behaviour, J. Catal. 423 (2023) 10–18.
[39] W.E. Lindsell, Magnesium, calcium, strontium and barium, in: E.W. Abel, F.G.A. Stone, G. Wilkinson (Eds.), Comprehensive Organometallic Chemistry, 1st ed., Elsevier, Pergamon, Oxford, 1982, pp. 155–252.
[40] N.D.R. Barnett, W. Clegg, R.E. Mulvey, P.A. O'Neil, D. Reed, Selective crystallization of di-sec-butylmagnesium. N, N, N', N'-tetramethylethylenediamine from solutions containing mixtures of normal-butyl and secondary-butyl isomers, J. Organomet. Chem. (1996) 297–300.
[41] C. Castán-Guerrero, D. Krizmancic, V. Bonanni, R. Edla, A. Deluisa, F. Salvador, G. Rossi, G. Panaccione, P. Torelli, A reaction cell for ambient pressure soft x-ray absorption spectroscopy, Rev. Sci. Instrum. 89 (2018).
[42] D.H. Simonne, A. Martini, M. Signorile, A. Piovano, L. Braglia, P. Torelli, E. Borfecchia, G. Ricchiardi, THORONDOR: a software for fast treatment and analysis of low-energy XAS data, J. Synchrotron. Radiat. 27 (2020) 1741–1752.
[43] F. Neese, F. Wennmohs, U. Becker, C. Riplinger, The ORCA quantum chemistry program package, J. Chem. Phys. 152 (2020).
[44] A.D. Becke, A new mixing of Hartree-Fock and local density-functional theories, J. Chem. Phys. 98 (1998) 1372.
[45] C. Lee, W. Yang, R.G. Parr, Development of the Colle-Salvetti correlation-energy formula into a functional of the electron density, Phys. Rev. B. 37 (1988) 785.
[46] F. Weigend, R. Ahlrichs, Balanced basis sets of split valence, triple zeta valence and quadruple zeta valence quality for H to Rn: design and assessment of accuracy, PCCP 7 (2005) 3297–3305.
[47] C. Van Wüllen, Molecular density functional calculations in the regular relativistic approximation: method, application to coinage metal diatomics, hydrides, fluorides and chlorides, and comparison with first-order relativistic calculations, J. Chem. Phys. 109 (1998) 392.
[48] L. Sementa, M. D'Amore, V. Barone, V. Busico, M. Causa', A quantum mechanical study of TiCl3α, β and γ crystal phases: geometry, electronic structure and magnetism, Phys. Chem. Chem. Phys. 11 (2009) 11264–11275.
[49] E. Borfecchia, L. Mino, E. Groppo, S. Bordiga, A.L. Bugaev, A. Budnyk, K.A. Lomachenko, A.A. Guda, M.A. Soldatov, A.V. Soldatov, C. Lamberti, Spectroscopic methods in catalysis and their application in well-defined nanocatalysts, Stud. Surf. Sci. Catal. (2017) 221–284.
[50] E. Groppo, E. Gallo, K. Seenivasan, K.A. Lomachenko, A. Sommazzi, S. Bordiga, P. Glatzel, R. Van Silfhout, A. Kachatkou, W. Bras, C. Lamberti, XAS and XES techniques shed light on the dark side of Ziegler-Natta catalysts: active-site generation, ChemCatChem 7 (2015) 1432–1437.
[51] M. Signorile, L. Braglia, V. Crocellà, P. Torelli, E. Groppo, G. Ricchiardi, S. Bordiga, F. Bonino, Titanium defective sites in TS-1: structural insights by combining spectroscopy and simulation, Angew. Chem. Int. Ed. 59 (2020) 18145–18150.
[52] A. Piovano, E. Morra, M. Chiesa, E. Groppo, Tuning the Ti3+ and Al3+ synergy in an Al2O3/TiClx catalyst to modulate the grade of the produced polyethylene, ACS Catal. 7 (2017) 4915–4921.
[53] K. Seenivasan, A. Sommazzi, F. Bonino, S. Bordiga, E. Groppo, Spectroscopic investigation of heterogeneous Ziegler-Natta catalysts: Ti and Mg chloride tetrahydrofuranates, their interaction compound, and the role of the activator, Chem. Eur. J. 17 (2011) 8648–8656.
[54] A. Piovano, K.S. Thushara, E. Morra, M. Chiesa, E. Groppo, Unraveling the catalytic synergy between Ti3+ and Al3+ sites on a chlorinated Al_2O_3: a tandem approach to branched polyethylene, Angew. Chem. Int. Ed. 55 (2016) 11203–11206.
[55] G. Takasao, T. Wada, A. Thakur, P. Chammingkwan, M. Terano, T. Taniike, Machine learning-aided structure determination for $TiCl_4$-capped $MgCl_2$ nanoplate of heterogeneous Ziegler-Natta catalyst, ACS Catal. 9 (2019) 2599–2609.
[56] T. Usami, S. Takayama, M. Yokoyama, EXAFS and XANES studies on MgCl2-supported Ziegler-Natta catalyst, J. Polym. Sci. 23 (1985) 427–432.
[57] G. Vlaic, J.C.J. Bart, W. Cavigiolo, A. Michalowicz, Fluorescence EXAFS of $MgCl_2$-Supported Titanium Trichloride, in: EXAFS and Near Edge Structure, Springer, Berlin, Heidelberg, 1983, pp. 307–309.
[58] C.K. Jorgensen, Absorption Spectra and Chemical Bonding in Complexes, first ed., Pergamon Press, 1962.
[59] B.J. Brisdon, T.E. Lester, R.A. Walton, Complex halides of transition metals-III* Electronic absorption spectra of hexahalotitanates(IV), vanadates (IV), and zirconates(IV), Spectrochim. Acta 23 (1967) 1969–1976.
[60] I. Pollini, Electronic transitions in α- and β-titanium trichloride, Solid State Commun. 47 (1983) 403–408.
[61] C.H. Maule, J.N. Tothill, P. Strange, J.A. Wilson, An optical investigation into the $3d^1$ and $3d^2$ transition-metal halides and oxyhalides, compounds near to delocalisation, J. Phys. C Solid State Phys. 21 (1988) 2153.
[62] G. Natta, P. Corradini, G. Allegra, Struttura cristallina della forma y del tricloruro do titanio, Rendiconti Dell'Academia Nazionale Dei Lincei Classe Di Scienze Fisiche, Matem. Natur. 26 (1959).
[63] A. Rimola, D. Costa, M. Sodupe, J.F. Lambert, P. Ugliengo, Silica surface features and their role in the adsorption of biomolecules: Computational modeling and experiments, Chem. Rev. 113 (2013) 4216–4313.
[64] J.P. Gallas, J.C. Lavalley, A. Burneau, O. Barres, Comparative study of the surface hydroxyl groups of fumed and precipitated silicas. 4. Infrared study of dehydroxylation by thermal treatments, Langmuir. 7 (1991) 1235–1240.
[65] A.G. Fisch, Effects of the ethoxide in the coordination sphere of titanium on the performance of $MgCl_2$-based Ziegler-Natta catalyst, Ind. Eng. Chem. Res. 57 (2018) 6141–6152.
[66] D. ho Lee, Y. tae Jeong, K. Soga, In situ formation of $mgcl_2$ support and internal donor during preparation of propylene polymerization catalysts, Ind. Eng. Chem. Res. 31 (1992) 2642–2647.
[67] K. Tangjituabun, S. Yull Kim, Y. Hiraoka, T. Taniike, M. Terano, B. Jongsomjit, P. Praserthdam, Effects of various poisoning compounds on the activity and stereospecificity of heterogeneous Ziegler-Natta catalyst, Sci. Technol. Adv. Mater. 9 (2008).
[68] N.N. Chumachenko, V.A. Zakharov, G.D. Bukatov, S.A. Sergeev, A study of the formation process of titanium–magnesium catalyst for propylene polymerization, Appl. Catal. A Gen. 469 (2014) 512–516.
[69] A. Thakur, P. Chammingkwan, T. Wada, R. Onishi, W. Kamimura, K. Seenivasan, M. Terano, T. Taniike, Solution-state NMR study of organic components of industrial Ziegler-Natta catalysts: Effect of by-products on catalyst performance, Appl. Catal. A Gen. 611 (2021).
[70] A. Zecchina, C. Otero Arean, Diatomic molecular probes for mid-IR studies of zeolites, Chem. Soc. Rev. 25 (1996) 187–197.
[71] A. Zecchina, D. Scarano, S. Bordiga, G. Spoto, C. Lamberti, Surface structures of oxides and halides and their relationships to catalytic properties, Adv. Catal. 46 (2001).
[72] C. Lamberti, A. Zecchina, E. Groppo, S. Bordiga, Probing the surfaces of heterogeneous catalysts by in situ IR spectroscopy, Chem. Soc. Rev. 39 (2010) 4951–5001.
[73] A. Piovano, J. Zarupski, E. Groppo, Disclosing the interaction between carbon monoxide and alkylated Ti3+species: a direct insight into Ziegler-Natta catalysis, J. Phys. Chem. Lett. 11 (2020) 5632–5637.
[74] E. Groppo, G.A. Martino, A. Piovano, C. Barzan, The active sites in the Phillips catalysts: origins of a lively debate and a vision for the future, ACS Catal. 8 (2018) 10846–10863.
[75] E. Groppo, C. Lamberti, S. Bordiga, G. Spoto, A. Zecchina, The structure of active centers and the Ethylene Polymerization mechanism on the Cr/SiO_2 catalyst: a frontier for the characterization methods, Chem. Rev. 105 (2005) 115–183.
[76] M.E.Z. Velthoen, A. Muñoz-Murillo, A. Bouhmadi, M. Cecius, S. Diefenbach, B. M. Weckhuysen, The multifaceted role of methylaluminoxane in metallocene-based olefin polymerization catalysis, Macromolecules 51 (2018) 343–355.
[77] V.N. Panchenko, I.G. Danilova, V.A. Zakharov, E.A. Paukshtis, An IR-spectroscopic study of the state of zirconiumin supported zirconocene catalysts, Kinet. Catal. 45 (2004) 547–553.
[78] H. Knozinger, Infrared spectroscopy as a probe of surface acidity, in: R.W. Joyner, R.A. van Santen (Eds.), Elementary Reaction Steps in Heterogeneous Catalysis, Kluwer Academic Publishers, 1993, pp. 267–285.
[79] G. Ghiotti, E. Garrone, C. Morterra, F. Boccuzzi, Infrared study of low temperature adsorption. 1. CO on aerosil. An interpretation of the hydrated silica spectrum, J. Phys. Chem. 83 (1979) 2863–2869.
[80] J.H. Teuben, E.J.M. De Boer, A.H. Klazinga, E. Klei, CO activation by dicyclopentadienyl derivatives of titanium, niobium and tantalum, J. Mol. Catal. 13 (1981) 107–114.
[81] R.B. Seymour, T. Cheng, Advances in Polyolefins The World's Most Widely Used Polymers, Springer, US, 1987.